Composite Structures 334 (2024) 117966

Contents lists available at ScienceDirect

Composite Structures

journal homepage: www.elsevier.com/locate/compstruct

Multi-stimulus responsive shape memory polyurea incorporating stress-mismatching structure for soft actuators and reversible deployable structures

Wen Liu [a], Deyan Kong [b,*], Wei Zhao [c], Jinsong Leng [a,*]

[a] National Key Laboratory of Science and Technology on Advanced Composites in Special Environment, Harbin Institute of Technology, Harbin 150080, People's Republic of China
[b] MIIT Key Laboratory of Critical Materials Technology for New Energy Conversion and Storage, School of Chemistry and Chemical Engineering, Harbin Institute of Technology, No. 92 West Dazhi Street, Harbin 150001, People's Republic of China
[c] Department of Astronautical Science and Mechanics, Harbin Institute of Technology (HIT), P.O. Box 301, No. 92 West Dazhi Street, Harbin 150001, People's Republic of China

ARTICLE INFO

Keywords:
Deployable structure
Shape memory
Reversible deformation
Bilayer actuator

ABSTRACT

Shape memory polymer (SMP) has demonstrated practical applications, including aerospace structures, medical devices, and flexible electronics. The programmability and controllability provide essential convenience for many device applications. Imperfectly, once a programmed temporary shape is deployed into a permanent shape, it cannot recover to the programmed shape without being reprogrammed. Here, through differential thermal expansion material synergistic design constructing stress-mismatching structure. The bilayer actuator is constructed, featuring excellent mechanical strength and toughness, responsive to light, humidity and electric field. The multi-dimensional cross layer of carbon material and intrinsic humidity response of shape memory polyurea (SMPU) is an active layer and PET is a passive layer. The bilayer actuator bends 140° within 5 s under 30 V voltage and recovers quickly within 20 s. Controlling the angle of light, the wheeled robot could crawl back and forth 20 cm, also achieving the bionic actuators, and deployable structures with an automatic roll-unfold.

1. Introduction

Stimuli-responsive materials, transforming their shape and functionality facing external stimuli, possess diverse applications including bio-inspired robots [1–3], soft manipulators [4,5], alarm actuating [6], protective equipment [7,8], and deployable solar arrays [9,10]. Shape memory polymer (SMP), a stimuli-responsive material with programmability, has been applied in the space deployable structure [11], deploy the national flag on Mars [12] through electricity, light, and magnetic field to trigger shape recovery with large deformation capability. Concentrating on studying SMP includes one-way, two-way, and multiple shape memory effect [13]. Then, one-way and multiple SMP have one or more temporary shapes with irreversible unidirectional recovery [14]. Compared with one-way SMP, two-way SMP is capable of reversible deformation between two despised shapes and consists of liquid crystal elastomers (LCEs) [15,16], and semi-crystalline polymers [17,18]. Deformation of LCEs depends on anisotropic-to-isotropic of mesogens, leading to contraction and expansion with only axial contraction and torsion without large area folding deformation ability [19,20]. Besides, semi-crystalline polymers have an ability of crystallization induced elongation and melting-induced contraction, but this demonstrate a small reversible strain so that it cannot be applied to large reversible deformation structure. Most SMP in deployable structures with a one-way shape memory effect, demonstrate that one program can only be expanded once at a time meaning that folding again requires reprogramming, which is difficult to accomplish on the space station [12]. Besides, two-way SMP will have a remarkable application in selective filtration, self-programmable window shades so that it is necessary to development of reversible actuators with rapid response to multiple stimuli [21,22].

Different from the deformation mechanism of SMP, a bilayer stimuli-responsive material is capable of reversible deformation based on unbalanced structural properties, such as the coefficient of expansion variance [23], and humidity-response [24,25]. The bilayer structure

* Corresponding authors.
E-mail addresses: dykong@hit.edu.cn (D. Kong), lengjs@hit.edu.cn (J. Leng).

https://doi.org/10.1016/j.compstruct.2024.117966
Received 16 October 2023; Received in revised form 14 January 2024; Accepted 6 February 2024
Available online 8 February 2024

consists of a passive layer and an active layer that is composed of by some electrical, light, and magnetic responsive materials, such as iodine-doping rGO/rGO [26], GO-CNT/PDMS [27], CNT/PC [28], and PEDOT:PSS/PDMS [29], which demonstrate high responsive sensitivity as well as reversibility. The bilayer structure can actively deform according to the set pattern under external stimuli, and also recover after removing external stimuli, mainly including bending and torsional deformation, such as a flower-shaped actuator [30], leaf-shaped actuator [29], and gripper actuator [26]. Specifically, bilayer actuators are mostly focused on an instinctive bending deformation based on an asymmetric expansion without preprogrammed temporary shape [31–33].

Therefore, integrating the programming of SMP with the reversible actuation of a bilayer structure, reversible responsive material is promising application in more convenient deployment structures. Herein, we construct an ingenious bilayer strategy for developing multi-responsive actuators applying in bionic actuators and deployment structures, which consist of three components: (1) intrinsic humidity response PU providing programmability. (2) 1D graphene and 2D carbon nanotubes interact to improve electrical conductivity. (3) PET as a passive layer to ensure unbalanced stimulus response behavior. The passive layer was inert to stimulus environment, converting the isotropic volume change to a macroscopic bending deformation [29]. The bilayer actuator possesses multiple stimulus-responsive capability and is triggered by humidity, electric field and simulated sunlight, attributing to humidity-responsive poly-hydroxyl and carboxyl groups, electric-thermal and photo-thermal of CNTs and GO. We demonstrate the application of the PU@CNTs-GO/PET bilayer actuator in bionic actuators (e,g., artificial flower, mimosa, wheeled robot, and wing of the butterfly) and programmed folding structures in spatial deployment structures by 300–2500 nm simulated sunlight, and a voltage limiter.

2. Experimental section

2.1. Materials

Poly(propylene glycol) bis(2-aminopropyl ether) (ED, Mn = 2000 g mol^{-1}), methylene-bis(4-cyclohexylisocyanate) (HMDI, 99 %), D-Tryptophan (DTP, 98 %) and N,N-dimethylacetamide (DMAc, 99.8 %), CNTs and nanographene sheets were purchased from Macklin (China). 1,3-Diamino-2-propanol (DMPP, 97 %) was purchased from Aladdin (China). PET was purchased from Shanghai Baixin Material Co. LTD.

2.2. Preparation of PU film

DMAc was drastically dried by the 4A molecular sieve about above 48 h, and ED2000 was dehydrated keeping 1 h at 120 °C in vacuum. Minutely, 50 wt% D2000(2.5 g) in DMAc was added into 50 wt% HMDI solution stirring acutely at room temperature for 0.5 h. Subsequently, the reaction solution was placed in ice bath with 7 wt% DMPP (0.7 g) in DMAc being added stirring 3 h. Then, 0.3 g DTP was added the reaction system stirring 24 h at room temperature. Finally, the reaction gunk was poured onto a glass plate and dried overnight to obtain light yellow PU film.

2.3. Preparation of the PU@CNTs-GO/PET bilayer actuator

Firstly, the active layer of ink was prepared. The ink was composed of equal GO nanoplates and CNTs (20 %), and PU (60 %) in DMAc stirring 48 h to a homogeneous black viscous liquid. Next, the ink was deposited by spin coating at a rate of 800 rpm for 30 s onto the PET film. The bilayer composite film was dried in the oven at 80 °C. Finally, a laser cutter cut the composite film into a set shape.

2.4. Characterization

Scanning electron microscope (SEM, SU5000) was employed to test the section of the bilayer actuator. Mechanical properties were characterized by the testing machine (SHIMADZU, AGS-X-10KN), and the strain rate was 30 mm/min at room temperature. Atomic Force Microscopy (AFM) was employed to character surface morphology in wet and dry state. The simulated sunlight source was 200–2500 nm (QFS2500).

3. Results and discussion

3.1. Structural analysis of PU film

Different from these composite materials by adding agarose, MXene, and cellulose to achieve humidity response [34,35], we fabricated an intrinsic humidity-responsive PU because of a large number of hydroxyl and carboxyl groups in the molecular structure. This preparation process was shown in Fig. 1a, firstly, through stepwise polymerization to get an isocyanate-sealed prepolymer, which continued to react with tryptophan. Owing to a large of tryptophan and the hydroxyl groups in the chain, the fabricated PU was super sensitive to moisture forming unbalanced intermolecular H-bonding resulting in macroscopic deformation. As shown in Fig. 1b, the film could quickly rolled up on the wet filter paper with recovering on a dry filter paper. This process corresponding to schematic diagram of microstructure change was shown in Fig. 1bii, and 1biv respectively, the absorbed water broken the H-bonding in PU molecules under water stimulus, while H-bonding would re-built under recovering to dry state and was reversibility. As shown in Fig. 1c, the pore size of the film in a dry state was completely different from a humidity state with an obvious increase. The pore was formed by the phase-separated structure, when the presence of water in the molecular network leading to a big expansion of phase separation nanostructures [36]. Moreover, the dynamic process of absorption and desorption was mapped in the change of weight along with time in Fig. 1d, demonstrating that unbalanced expansion could be reversibly transformed only by variation of relative humidity. Multistage H-bonding could improve polymer strength and toughness resulting high strength and ductility of PU in Fig. 1e, because H-bonding as non-covalent sacrificial bonds was capable of extending the local damage at the crack tips to the entire polymer network to achieve energy dissipation and absorption [37,38]. Particularly, the H-bonding was broken when the PU film was exposed in moisture leading that strength of PU molecular network was weakened and the ductility was increased. Water molecules break the original intermolecular H-bonding cross-linked network in Fig. 1bii, and form slippable intermolecular H-bonding with side chain —OH and —COOH in Fig. 1biv, increasing the ductility of PU. From microstructure to mechanical properties to macroscopic deformation, it was fully demonstrated that the PU film was super sensitive to humidity. Herein, it was expected that PU film had ultra-sensitive human humidity response, and could bend quickly when finger closed, when finger was removed, it enabled recover original state reversibly (Fig. S1), and we could see clearly from Fig. S2 that there was no obvious deterioration of bend-recovery curves after 30 cycles.

3.2. Structure of the actuator

Different from traditional SMP with one-way effect, this actuator was composed of active/passive two layers of films with a reversible effect. In Fig. 2a, the preparation process was that the conductive ink was evenly coated onto PET film. An active layer of the conductive ink with humidity response, was constructed by a multi-dimensional structure of thermal materials and shape memory PU. The conductive ink, a black viscous liquid (PU@CNTs-GO) was shown in Fig. 2b, and the molecular network consisted of 1D GO nanosheets, 2D CNTs, and a polyhydric PU network terminated by tryptophan with carboxyl to improve humidity responsive sensitivity in Fig. 2c. Cross-sectional SEM image of PU@CNTs-GO active film had a dense and ordered layered structure, featuring of PU as “concrete” between CNTs-GO without visible gaps or voids in Fig. 2e. Besides, the uniform distribution of C, and O elements

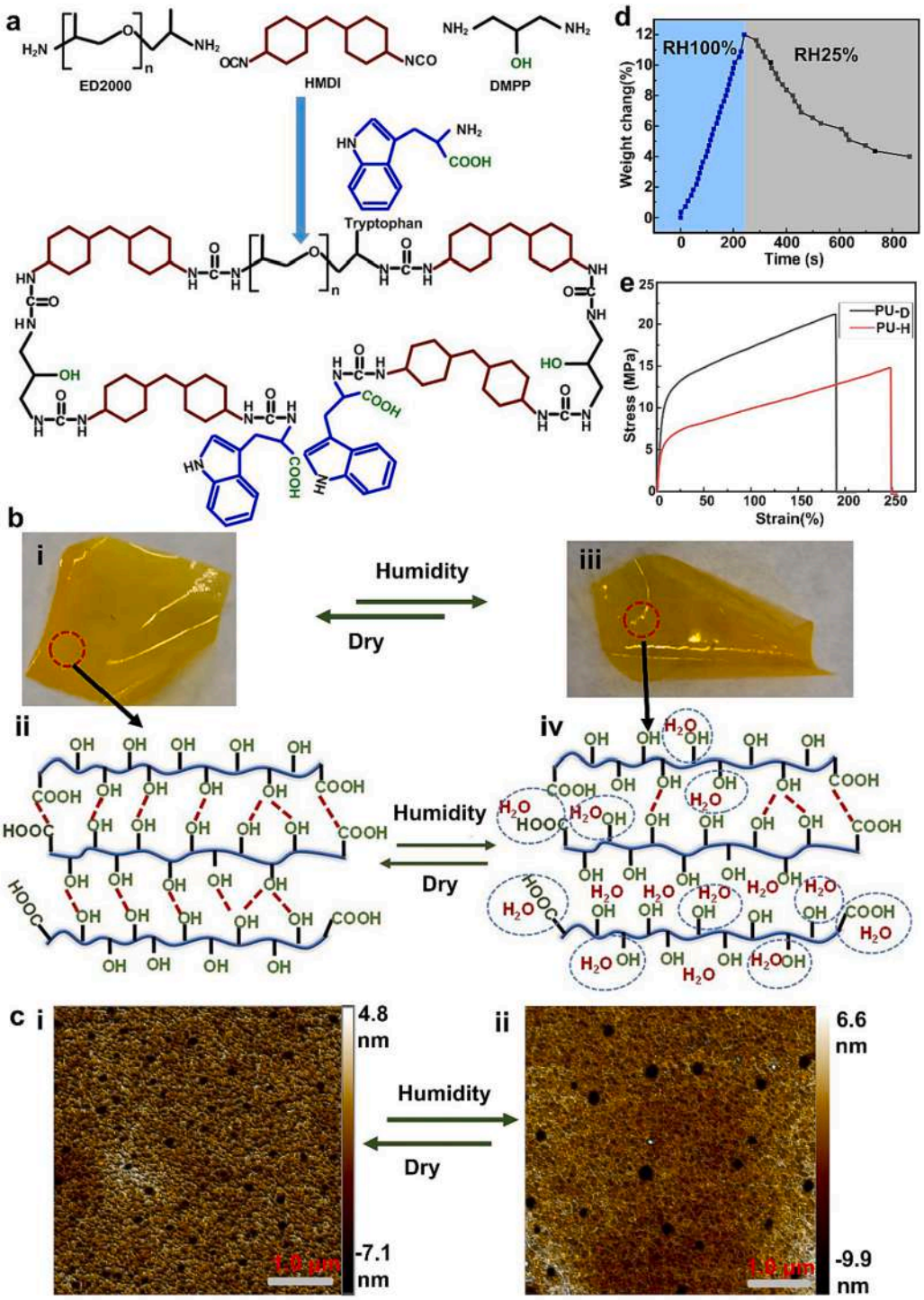

Fig. 1. (a) Chemical structure of humidity-responsive PU. (b) Macroscopic deformation of the film before (i) and after (ii) exposure to high humidity corresponding molecular structure (ii) and (iv). (c) Microscopic structural changes of the film in dry (i) and exposure humidity air (ii). (d) Variation of the weight of the film under RH 100 % and 25 % air. (e) Comparison of stress–strain curves with dry and soaked-12 h in water.

the was presented by energy dispersive spectroscopy (EDS) without obvious aggregates in Fig. 2f, indicating evenly dispersed CNTs-GO nanoparticles [35]. The actuator had great flexibility and foldability in Fig. 2d. Section microstructure of the two-phase film was shown in Fig. 2g, clearly, the thickness of a passive and active layer was 0.04 μm, and 0.01 μm, respectively. A thin active layer benefited to improve the rapid sorption/desorption of humidity and expansion/flattening of heating [29].

3.3. Deformation mechanism of the actuator

The bilayer actuator was composed of two materials with unbalanced thermal expansion coefficients that was the foot of driving force. Specifically, the deformation mechanism was shown in Fig. 3a under different stimulus conditions. The active layer was particularly sensitive to humidity because of a large number of —OH and —COOH that could absorb water to expand resulting in increasing of the distance between molecules, while the volume of the PET layer remained basically

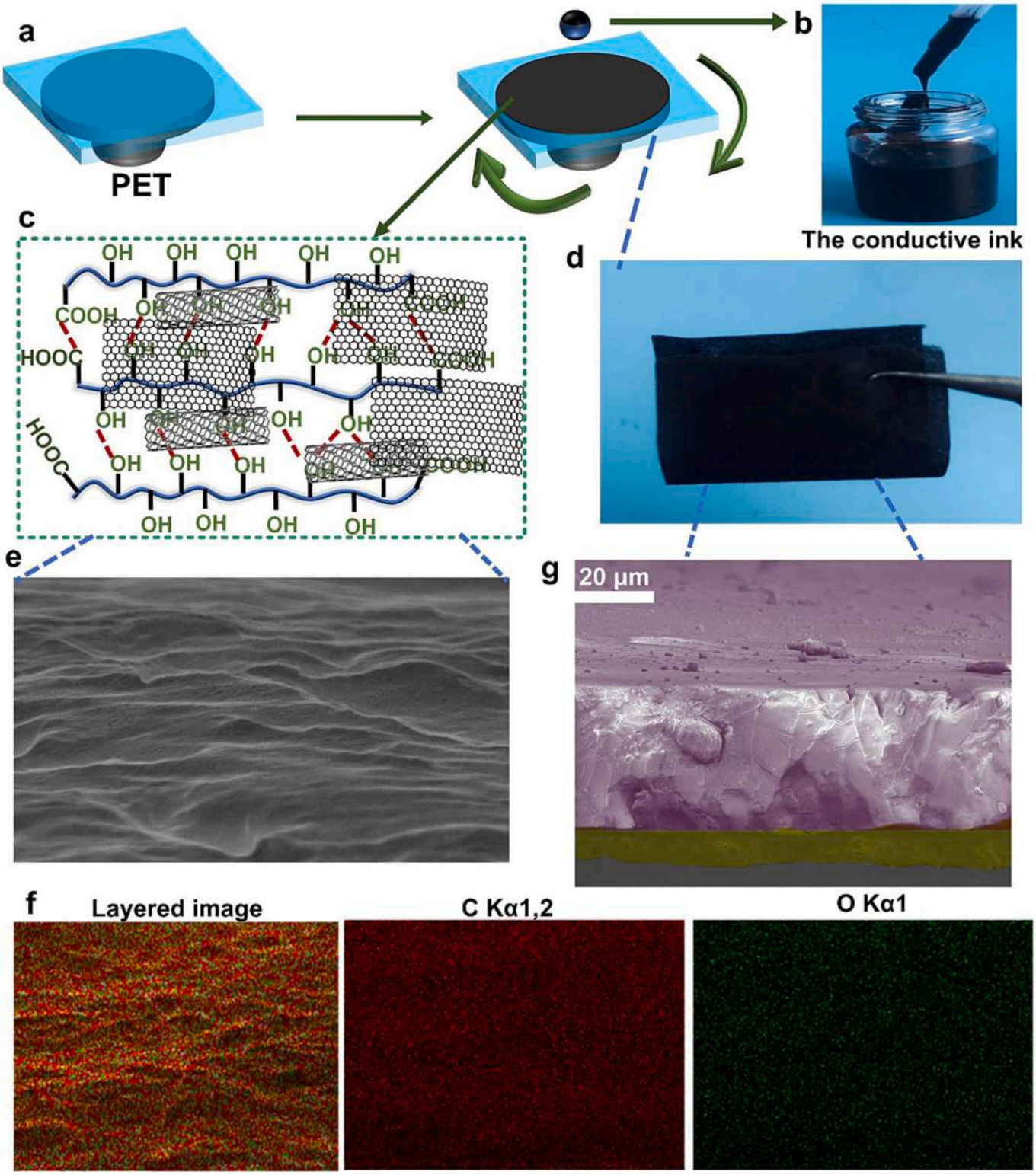

Fig. 2. (a) Preparation process of the actuator. (b) Ropy conductive ink. (c) Molecular network structure of conductive ink. (d) The folded state of actuator. (e) SEM image of PU@CNTs-GO active film. (f) Corresponding EDS image. (g) Sectional microstructure of the actuator.

unchanged, and the closely connected two layers naturally bend in Fig. 3i. In contrast, in response to thermal stimulation in Fig. 3ii, the molecular chains of the active layer shrink and CNTs-GO had a smaller coefficient of thermal expansion than PET, so a natural bend occurred. Further, because the varying degrees of volume expansion and segment contraction were physical changes, and when the stimulus was removed, those changes would automatically recover. For example, whenever it came to electric fields, light, the active layer was triggered to produce contraction, leading to bending deformation toward an active layer, and the bending deformation was reversible along with the flattening of expansion in Fig. 3b. Demonstrably, in Fig. 3c, a simple pattern was triggered to bend nearly 180° under applying a 30 V voltage,

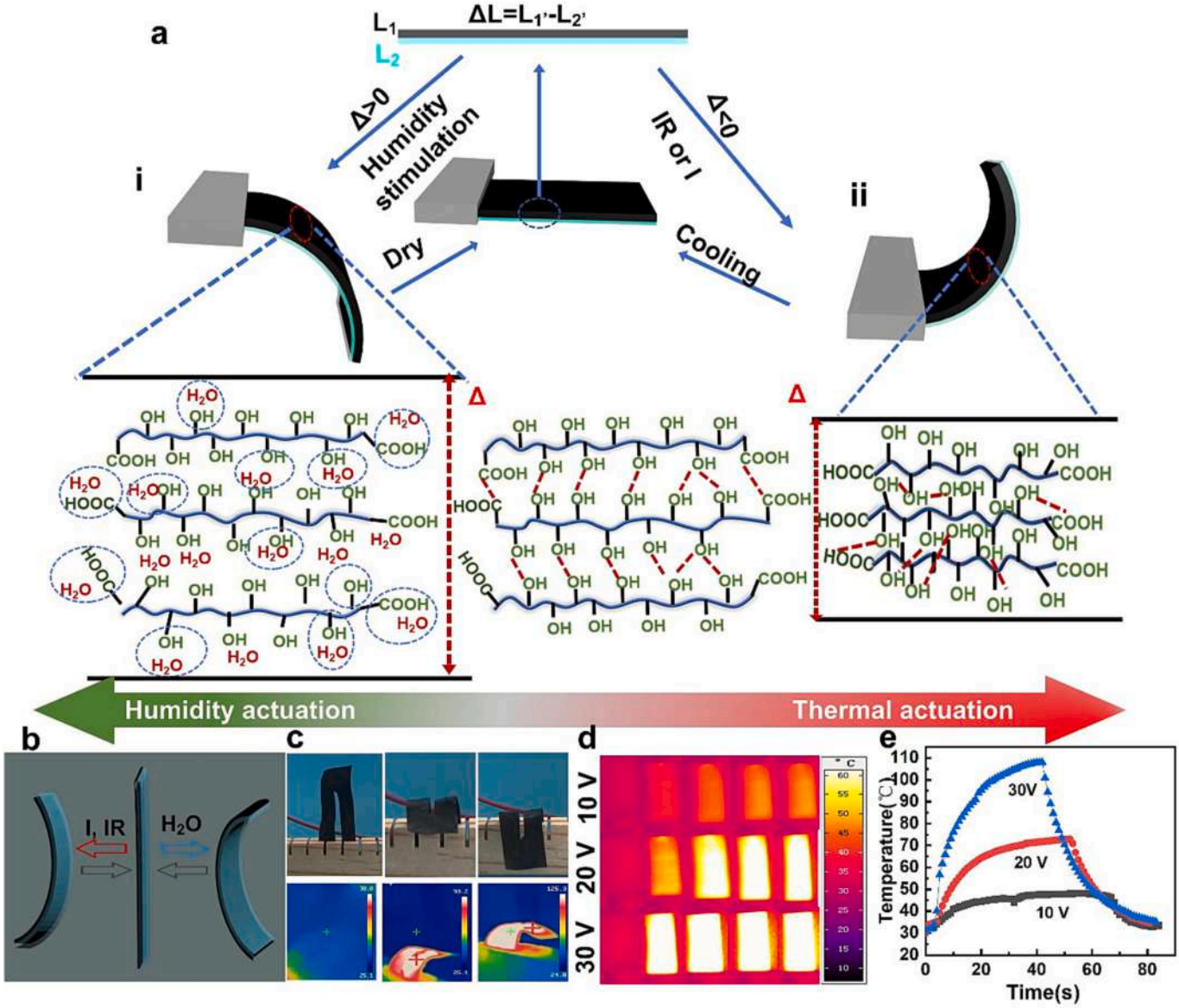

Fig. 3. (a) Mechanism of reversible deformation of actuator. (b) Bending direction under different stimuli. (c) An electrically driven bending deformation and corresponding IR thermal image. (d) IR thermal image under different voltage. (e) Temperature variation curve with time.

corresponding uniform IR thermal image along the current in Fig. 3d. Further, combined with IR imaging and temperature variation, the thermal uniformity and response rate of the actuator were investigated. Obviously, the IR thermal imaging of the actuator was uniform owing to no phenomenon of only local heat, and the surface temperature increased with the increase of voltage, corresponding to temperature curve with time along with fast rate of heating and cooling in Fig. 3f.

3.4. Electric-thermal actuation performance of the actuator

PU@CNTs-GO, an active layer with a stable mud-brick structure had excellent electric-thermal. To investigate the electrical response performance of the actuator, we designed a beam-shaped structure, and researched actuation performance influence corresponding different beam-shape structure. As shown in Fig. 4a, the actuator was able to quickly bend to 140° applying 30 V voltage within 7 s with a deformation rate of 20°/s that was 4 times the recovery rate of SMP by heating [39], which indicated that the actuator had a large bending deformation ability and fast response performance. Notably, this bending angle was capable of automatic recovery with a recovery rate of 96 % when removing a voltage (Movie S1), because part of the molecular chain was permanently deformed leading not 100 % recovery. As shown in Fig. 4b, when the voltage was off, the actuator was capable of recovering to the original within 14 s, which was reversible, controllable, and different from a one-way shape memory actuator only programming loops one at a time. The current flow direction directly affected the actuation performance of the actuator, so three beam structures were prepared (namely S1, S2, and S3) with the same dimensions (5 mm wide, 35 mm long) but different beam width (5, 10, and 15 mm, respectively) to demonstrate actuation performance difference. Minutely, three kinds beam width was shown in Fig. 4c. When applying same 20 V voltage, the surface temperature S1, S2 and S3, was 32, 40, and 70 °C respectively. When applying same 30 V voltage, the surface temperature S1, S2 and S3, was 70, 90, and 120 °C respectively, which indicating that S3 had highest electric-thermal effect due to minimum resistance. PU had excellent thermal stability with minimum thermal decomposition temperature of 226 °C (Fig. S3) to ensure stable operation at 120 °C. The difference of temperature directly affected the deformation ability. As shown in Fig. 4d, the bending rate and recovery rate of S1, S2, and S3 were evaluated by applying 30 V voltage.

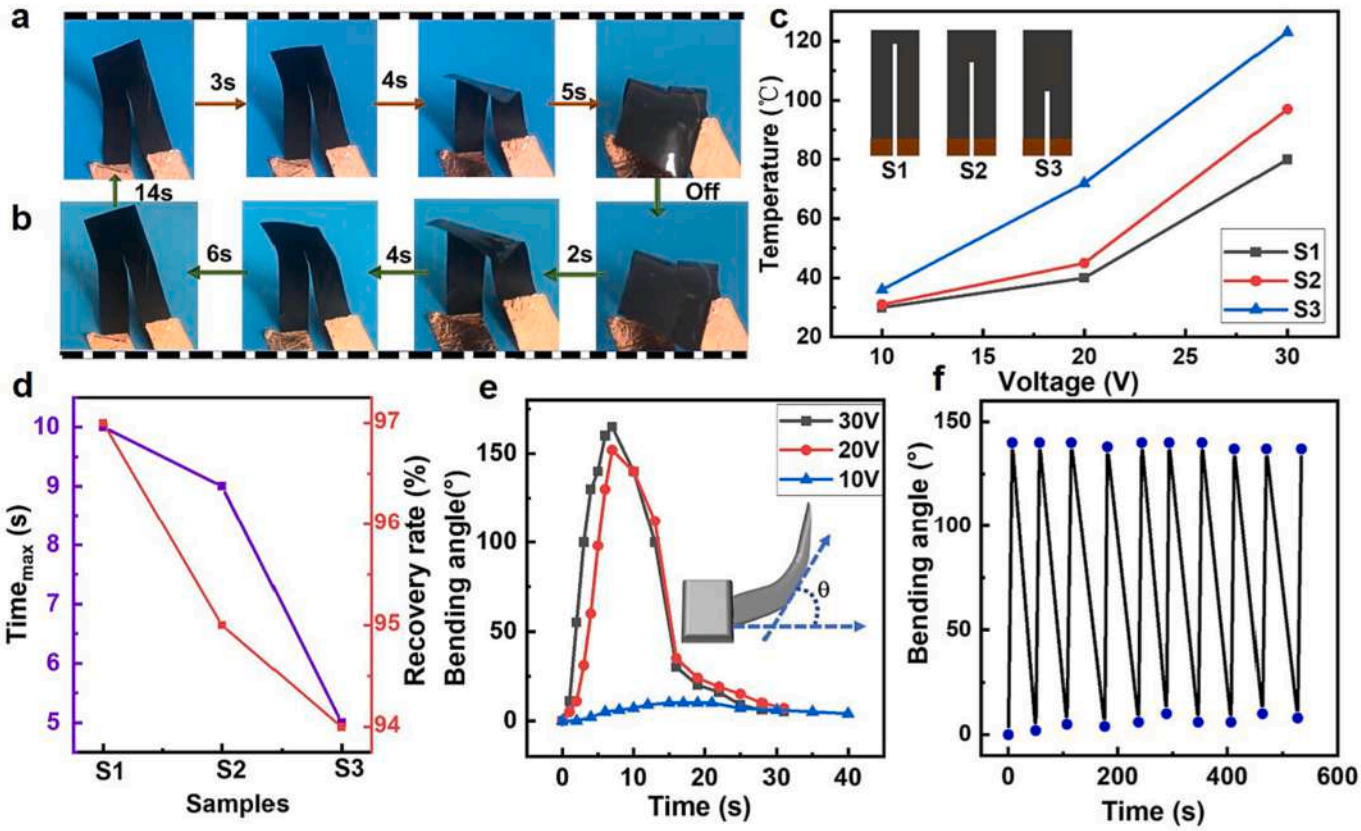

Fig. 4. (a) The bending deformation of the actuator applying an electric field. (b) The recovery process of the actuator removing an electric field. (c) The surface temperature of the three samples under different voltages. (d) Controlling constant deformation 140°, deformation time and recovery rate of three samples under 30 V voltage. (e) Bending angle of S2 under different voltages. (f) Repeatability test under 30 V voltage.

Maintaining the same bending angle of 140°, the bending rate of S1, S2, and S3 was 14, 20, and 28°/s, which indicating that S3 had the fastest response speed due to most excellent electrothermal effect. However, the recovery rate of S1, S2, and S3 was 97 %, 96.5 %, and 94 %, and S3 had the lowest recovery rate because the high temperature could cause irreversible deformation of the chain segments. By comprehensive comparison, S2 has a suitable response performance. Hence, the influence of voltage on S2 actuation performance was analyzed systematically in Fig. 4e. Applying 10 V voltage generated a temperature of 30 °C leading to small expansion imbalance with a bending of below 10°, which indicated that the temperature of below 30 °C could triggered the actuator.

Increasing to 20 V could generate about 40 °C temperature, and triggered a bending angle of 140° within 7 s. The removal of voltage enabled the bending angle to recovery an original state, which indicating that the actuator could be driven at a lower temperature. Applying a 30 V voltage generated about 90 °C, and triggered a bending angle of 170° within 9 s, which demonstrated that the increase in voltage would cause the bending speed and angle to increase. As shown in Fig. 4f, bending and recovery of the actuator was reversible and repeatable stability.

3.5. Potential applications in bionic actuators

Controllable deformation ability along with the customizability of drive pattern and deformation path made it possible to achieve a variety of deformation applications for bioinspired active structures possessing perception and actuation capabilities. For electrical-driven actuator, the specific deformation path depended on the current flow direction. Just like a night flower with the future of closing during the day and blooming at night, the flower actuator converted a drooping petal state into a closed petal state under electric field stimulation in Fig. 5a, but the deformation was not ideal because complex path. Analogously, a mimosa actuator was demonstrated in Fig. 5b, when was stimulated by an electric field, achieve close to 60° of protective contraction just 3 s like a mimosa, and deformation stability after 8 s. However, because the paths were not exactly the same, the amount of contraction was not the same, demonstrating that the actuator was not suitable for complex deformation when driven by electric field. Some simple bending deformations can be used as smart sensors, such as a voltage-limiting protective part [40]. As shown in Fig. 5c, a 20 V voltage-limiting protective part was demonstrated, when the inflow voltage above 20 V, the overvoltage circuit was connected to triggered the bilayer actuator to bend, which signal was received by a sensor to send an alarm; when the voltage was lower 20 V, the bilayer could not bend without object covered sensors. Inversely, the alarm would be triggered with inflow voltage of above 20 V owing to bending of bilayer covering the sensor. Thus, the bilayer actuator can be a new approach to apply in warning device overvoltage circuit.

Different from the electric-driven actuator with single deformation, light-driven actuator could achieve complex deformation. To demonstrate the dexterous deformation of the bilayer actuator by light, we simulated some bionic structures for verification. The chameleon's tongue can stretch to twice its own length in as little as 70 ms, taking down prey quickly and accurately [41]. As shown in Fig. 6a, we fabricated a 5 cm-retroflex bilayer actuator with a structure of the active layer in outer layer to simulate the chameleon's tongue. The retroflex bilayer actuator could quickly tongue with 20 mm just 6 s applying an NIR laser (0.5 W/cm^2), and automatically shrink to crimp state just 3 s after removing NIR laser (Movie S2), which was promising in soft crimp robots. The outer active layer was contracted by the photo-thermal effect, showing a flattening deformation trend, resulting in the extension

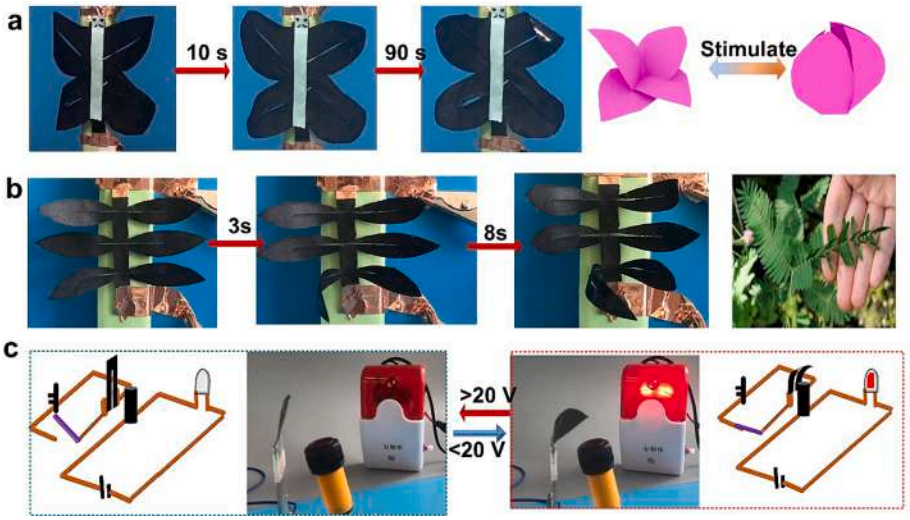

Fig. 5. (a) Closure – blooming flower-shaped actuator. (b) Mimosa-shaped actuator. (c) Schematic diagram of a 20 V voltage-limiting protective part.

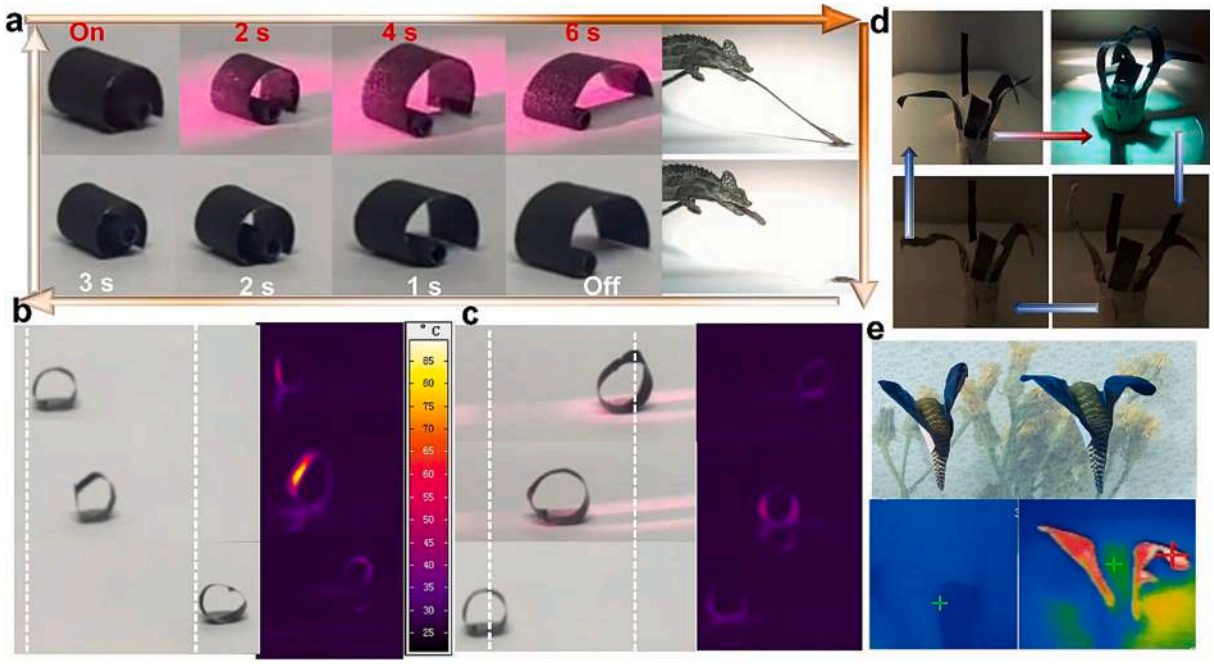

Fig. 6. (a) retractile actuator like chameleon tongue by nir drive. (b and c) The process photographs and ir thermal images of the wheel robot. (d) Closure – blooming flower applying simulated sunlight. (e) Butterfly-shaped actuator corresponding IR thermal images.

of the soft crimp robots. Besides, we designed a wheel robot that could move forward or backward by intermittently changing the direction of NIR laser. When the incident angle of IR light was 45°, the top of the wheel was subjected to thermal contraction producing centripetal force to push the wheel forward 30 mm only 22 s in Fig. 6b. On the contrary, when the incident angle of photo was −45°, the wheel robot could reverse motion back to the starting point in Fig. 6c (Movie S3), which indicating that the development of intelligent wheeled robots was possible by reasonable design and precise control of the surrounding environment. Many plants in nature can sense external stimuli to regulate their flower petals. For example, a flower-shaped actuator in Fig. 6d, closed fleetly beyond 90° deformation within 5 s applying a simulated sunlight, when sunlight was off, the actuator recovered to its original blooming shape only 21 s, which simulated a closing – blooming deformation process (Movie S4). A constant switch to control sunlight enabled the actuator like a butterfly to keep fluttering wings in Fig. 6e, similar to the deformation mechanism of electric-thermal that thermal stimulation triggered the unbalanced phase change [42,43]. Compared with applying an electric field, sunlight was more convenient, and the actuator shape was not limited, which improved potential application value in soft biomimetic robot.

3.6. *Reversible actuation incorporating programmability of SMPU*

The advantage of SMP is programmable property that fixed a specific temporary shape adapting to the complex environments and enable it to recover original shape byapplying a specific stimulus, which were demonstrated in biomimetic intestinal stents [44], aerospace field [45]. A typical one-way shape memory process was shown in Fig. 7a, the bilayer actuator was fixed into a rolled-up temporary shape, recovering to the original shape by heating, but it could not recover again temporary shape, which was restricted by programming one loop at a time. A

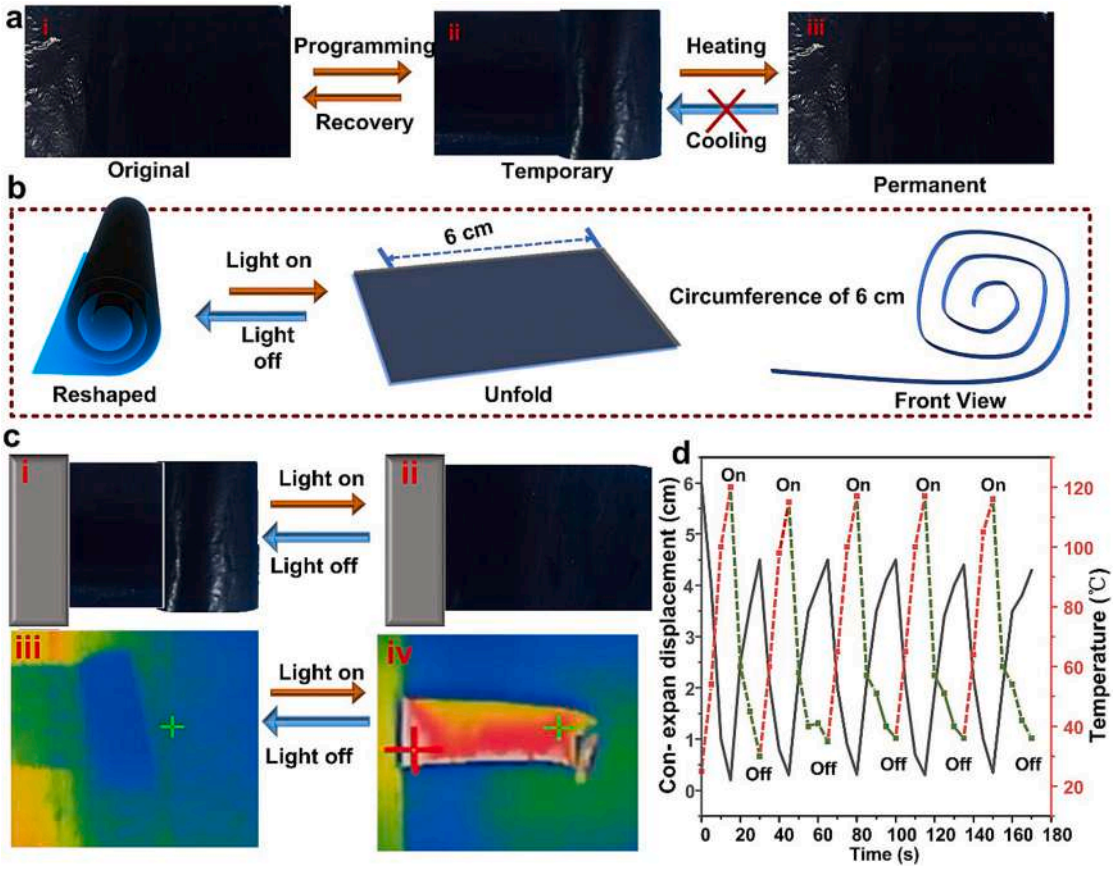

Fig. 7. (a) A programming process of one-way shape memory effect. (i) Original shape of single-layer PU composite film. (ii) Programming temporary shape. (iii) Recovery to permanent shape. (b) Structure diagram of bilayer actuator and circumference of deformation. (c) Reversible driving of bilayer actuator. (i) The folded state of programming, and (ii) unfolded state with a light on, corresponding IR image (iii) and (iv). (d) Five cycles curve of displacement and temperature as time.

breakthrough, integrating the reversible actuation of the bilayer actuator and shape memory programmability of PU, overcame the defects of irreversible of one-way shape memory effect and the problems of bilayer actuation without programmability. To better understand the programming process and structure of the bilayer actuator, a model diagram was presented in Fig. 7b. Notably, the green represented a passive layer, while the active layer was programmed into the outer layer with a 6 cm long rectangle rolled into a cylinder. As shown in Fig. 7c, rolled-up shape was smoothly deployed to 6 cm only 40 s with a flattening speed of 1.2 mm/s in Fig. 7cii. Definitely, when the simulated sunlight was off, the bilayer was able to recover the original rolled-up shape only 24 s with a recovery speed of 2.5 mm/s, and the process could continue all the time only by controlling a light source switch. Corresponding to the IR thermal image in Fig. 7ciii and civ, simulated sunlight generated 120 °C to trigger the active layer to unfold (Movie S5). To demonstrate the deformation ability and stability of the actuator, five cyclic tests were in Fig. 7d. The rolled up actuator was nearly 100 % flattened, and the recovery volume was basically stable at 4.5 cm. Generally, the bilayer actuator possessed a two-way shape memory effect with large deformation, quick response, and being remotely triggered by sunlight, which was possible to apply in space deployable structure.

3.7. Future application concepts in space deployable structure

The reversibility, photothermal-driven and stability of the actuator had been discussed, and we established some application models. For a deployable structure of space and the lunar surface, the intensity of sunlight could provide enough photo-thermal effect to trigger the bilayer actuator to deploy [12]. As shown in Fig. 8a, the bilayer actuator was designed to a folded flag state, and the flag was unfolded when exposed to the light, applying in the lunar surface flag unfolding structure (Movie S6), which did not require any additional mechanical force to drive. Similarly, the bilayer actuator simulated a satellite flexible solar panel. Theoretically, when a satellite was in the sunlight, the flexible wing structure would unfold to carry out work and be able to tighten in the absence of sunlight. Diversely, in Fig. 8b, the bilayer actuator was fixed directly to one end of the solar panel without pre-programmed shape. Then, the active layer expanded to roll up when stimulated by light, so that solar panels normally receive sunlight to generate electricity. Finally, the bilayer was very promising in dustproof for solar panel battery of Mars rovers because this structure did not require complex structural design and bearing capacity calculation like satellite flexible solar panel. As we all know, the rover would deposit a lot of dust, affecting its power generation efficiency. The bilayer actuator would lay flat on the solar panel to shield it from dust without sunlight, and roll up and take away the dust without affecting the solar panel work when there was sunlight, which demonstration process was shown in Figs. S2 and S3. In conclusion, the actuator as a reversible ingenious structure, achieved remote controllable deformation just by making proper use of sunlight.

4. Conclusion

Aiming at extending the one-way shape memory effect for reversible deformation, we designed a multi-stimulus responsive bilayer actuator, with excellent sensitivity to electricity, simulated sunlight/infrared light, and humidity. Applying a 30 V voltage, the bilayer actuator was capable of bending 140° within 5 s and achieving deformation of some bioinspired structures by designing the path of the current, such as tuberose, and mimosa. When the temperature was above 40 °C, the

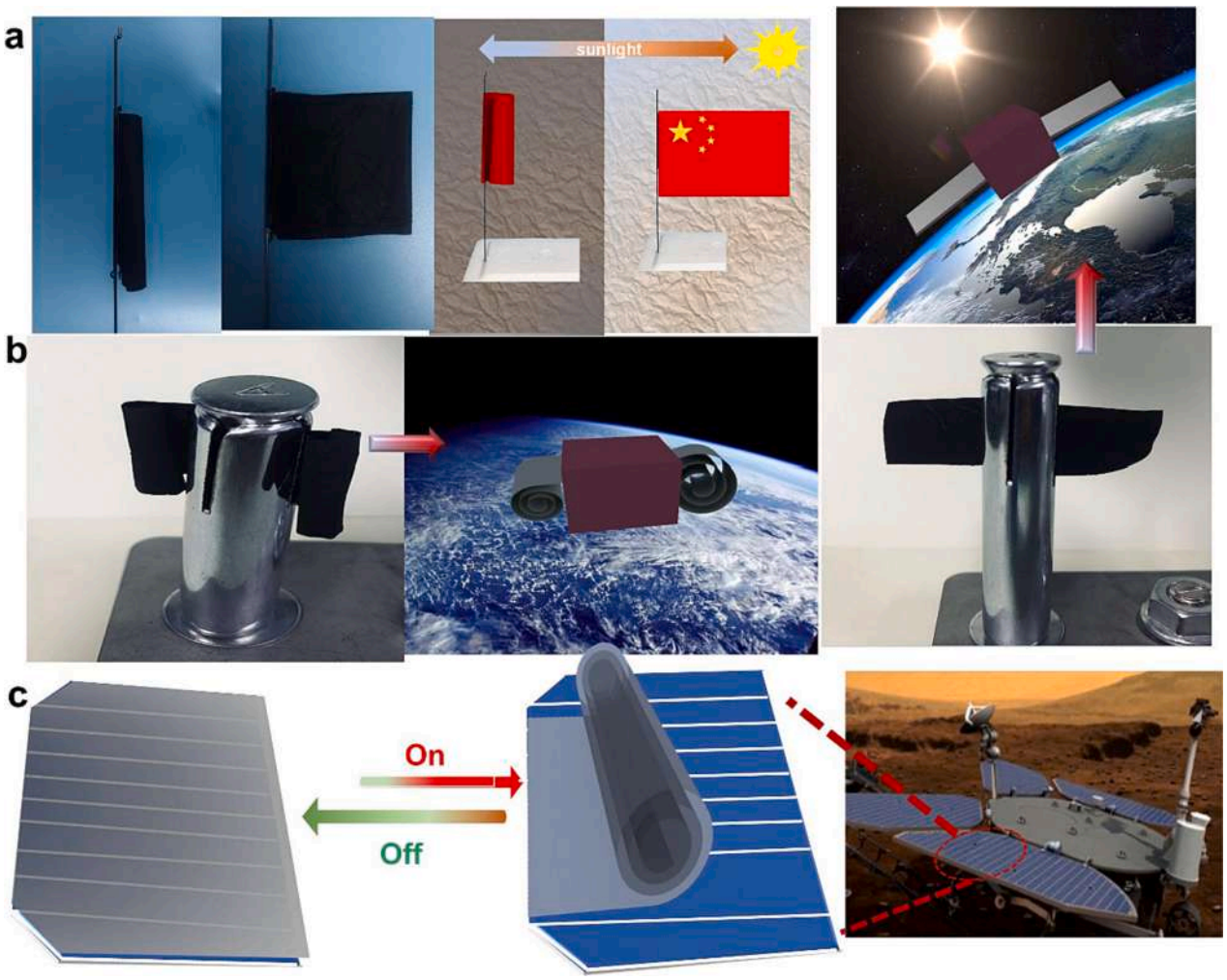

Fig. 8. Future application concepts of (a) flag unfurling, (b) and flexible solar array systems, and (c) automatically deploy-tighten a solar array dustproof film.

bilayer actuator could be activated to bend 140°. Simulated sunlight was able to trigger the bilayer to bend toward the light source, and by controlling the light source, it could open and close like a flower, stir its wings like a butterfly, retractile actuator like a tongue of a chameleon and a wheel robot, which was used in bionic actuator. Combining the programmability of SMPU with the reversibility deformation of the bilayer actuator, a series of deployable structures were demonstrated. The actuator as a reversible ingenious structure, achieved remote controllable deformation just by making proper use of sunlight, which was promising in the spatial deployable structure, especially in Mars rover intelligent dustproof film.

CRediT authorship contribution statement

Wen Liu: Data curation, Investigation, Methodology, Visualization, Writing – original draft, Writing – review & editing. **Deyan Kong:** Investigation, Methodology, Project administration, Resources, Validation, Writing – review & editing. **Wei Zhao:** Investigation, Methodology, Validation, Writing – review & editing. **Jinsong Leng:** Conceptualization, Funding acquisition, Project administration, Supervision, Writing – review & editing.

Declaration of competing interest

The authors declare that they have no known competing financial interests or personal relationships that could have appeared to influence the work reported in this paper.

Data availability

Data will be made available on request.

Acknowledgements

This research was supported by the National Key R&D Program of China (No. 2022YFB3805700).

Appendix A. Supplementary material

Supplementary material to this article can be found online at https://doi.org/10.1016/j.compstruct.2024.117966.

References

[1] Yu Y, Su Z, Chen W, Yang Z, Yang K, Meng F, et al. Electro-thermally driven biaxial bending artificial muscle based on oriented graphite nanoplate nanocomposite/polyimide complex structure. Compos Part A Appl Sci Manuf 2022;163:107164.
[2] Ilami M, Bagheri H, Ahmed R, Skowronek EO, Marvi H. Materials, actuators, and sensors for soft bioinspired robots. Adv Mater 2021;33(19).
[3] Li C, Peng ZK, He Q. Stimuli-responsive metamaterials with information-driven elastodynamics programming. Matter 2022;5(3):988–10034.
[4] Shintake J, Rosset S, Schubert B, Floreano D, Shea H. Versatile soft grippers with intrinsic electroadhesion based on multifunctional polymer actuators. Adv Mater 2016;28(2):231–85.
[5] Shian S, Bertoldi K, Clarke DR. Dielectric elastomer base "grippers" for soft robotics. Adv Mater 2015;27(43):6814–9.
[6] Wang K, Zhang T, Li C, Xiao X, Tang Y, Fang X, et al. Shape-reconfigurable transparent wood based on solid-state plasticity of polythiourethane for smart

building materials with tunable light guiding, energy saving, and fire alarm actuating functions. Compos B Eng 2022;246:110260.
[7] Hu W-H, Ji M, Chen T-T, Wang S, Tenjimbayashi M, Sekiguchi Yu, et al. Light-induced topological patterning toward 3D shape-reconfigurable origami. Small 2022;18(14).
[8] Liu He, Liu R, Chen K, Liu Y, Zhao Y, Cui X, et al. Bioinspired gradient structured soft actuators: from fabrication to application. Chem Eng J 2023;461:141966.
[9] Liu Y, Pan F, Xiong F, Wei Y, Ruan Y, Ding B, et al. Ultrafast shape-reconfigurable chiral mechanical metamaterial based on prestressed bistable shells. Adv Funct Mater 2023;33(25).
[10] Zhang D, Liu L, Leng J, Liu Y. Ultra-light release device integrated with screen-printed heaters for CubeSat's deployable solar arrays. Compos Struct 2020;232:111561.
[11] Wang X, He Y, Liu Y, Leng J. Advances in shape memory polymers: remote actuation, multi-stimuli control, 4D printing and prospective applications. Mater Sci Eng R Rep 2022;151:100702.
[12] Zhang D, Liu L, Xu P, Zhao Y, Li Q, Lan X, et al. World's first application of a self-deployable mechanism based on shape memory polymer composites in Mars explorations: ground-based validation and on-Mars qualification. Smart Mater Struct 2022;31(11):115008.
[13] Xia YL, He Y, Zhang FH, Liu YJ, Leng JS. A review of shape memory polymers and composites: mechanisms, materials, and applications. Adv Mater 2021;33(6).
[14] Huang X, Fu J, Tan H, Miu Y, Xu M, Zhao Q, et al. Molecular movements of trehalose inside a single network enabling a rapidly-recoverable tough hydrogel. Int J Smart Nano Mater 2022;13(4):575–96.
[15] Jiang X, Tian B, Xuan X, Zhou W, Zhou J, Chen Y, et al. Cellulose membranes as moisture-driven actuators with predetermined deformations and high load uptake. Int J Smart Nano Mater 2021;12(2):146–56.
[16] Zhai F, Feng Y, Li Z, Xie Y, Ge J, Wang H, et al. 4D-printed untethered self-propelling soft robot with tactile perception: rolling, racing, and exploring. Matter 2021;4(10):3313–26.
[17] Li J, Rodgers WR, Xie T. Semi-crystalline two-way shape memory elastomer. Polymer 2011;52(23):5320–5.
[18] Zhou J, Turner SA, Brosnan SM, Li Q, Carrillo J-M, Nykypanchuk D, et al. Shapeshifting: reversible shape memory in semicrystalline elastomers. Macromolecules 2014;47(5):1768–76.
[19] Chen GC, Jin BJ, Shi YP, Zhao Q, Shen YQ, Xie T. Rapidly and repeatedly reprogrammable liquid crystalline elastomer via a shape memory mechanism. Adv Mater 2022;34(21).
[20] Gelebart AH, Jan Mulder D, Varga M, Konya A, Vantomme G, Meijer EW, et al. Making waves in a photoactive polymer film. Nature 2017;546(7660):632–6.
[21] Zhao F, Zheng XY, Zhou SC, Zhou B, Xue SF, Zhang Y. Constitutive model for epoxy shape memory polymer with regulable phase transition temperature. Int J Smart Nano Mater 2021;12(1):72–87.
[22] Zare M, Prabhakaran MP, Parvin N, Ramakrishna S. Thermally-induced two-way shape memory polymers: mechanisms, structures, and applications. Chem Eng J 2019;374:706–20.
[23] Chen PN, He SS, Xu YF, Sun XM, Peng HS. Electromechanical actuator ribbons driven by electrically conducting spring-like fibers. Adv Mater 2015;27(34):4982–8.
[24] Opdenbosch DV, Popovski GF, Wagermaier W, Paris O, Zollfrank C. Moisture-driven ceramic bilayer actuators from a biotemplating approach. Adv Mater 2016;28(26):5235–40.
[25] Wani OM, Verpaalen R, Zeng H, Priimagi A, Schenning APHJ. An artificial nocturnal flower via humidity-gated photoactuation in liquid crystal networks. Adv Mater 2019;31(2).
[26] Yang J, Zhang J, Li X, Zhou J, Li Y, Wang Z, et al. Single janus iodine-doped rGO/rGO film with multi-responsive actuation and high capacitance for smart integrated electronics. Nano Energy 2018;53:916–25.
[27] Wang W, Xiang CX, Zhu Q, Zhong WB, Li MF, Yan KL, et al. Multistimulus responsive actuator with GO and carbon nanotube/PDMS bilayer structure for flexible and smart devices. ACS Appl Mater Interfaces 2018;10(32):27215–23.
[28] Zhang X, Yu Z, Wang C, Zarrouk D, Seo J-W, Cheng JC, et al. Photoactuators and motors based on carbon nanotubes with selective chirality distributions. Nat Commun 2014;5(1).
[29] Taccola S, Greco F, Sinibaldi E, Mondini A, Mazzolai B, Mattoli V. Toward a new generation of electrically controllable hygromorphic soft actuators. Adv Mater 2015;27(10):1668–75.
[30] Kim H, Lee H, Ha I, Jung J, Won P, Cho H, et al. Biomimetic color changing anisotropic soft actuators with integrated metal nanowire percolation network transparent heaters for soft robotics. Adv Funct Mater 2018;28(32).
[31] Ji MY, Jiang N, Chang J, Sun JQ. Near-infrared light-driven, highly efficient bilayer actuators based on polydopamine-modified reduced graphene oxide. Adv Funct Mater 2014;24(34):5412–9.
[32] Wang CW, Wang YB, Yao YG, Luo W, Wan JY, Dai JQ, et al. Solution-processed high-temperature, flexible, thin-film actuator. Adv Mater 2016;28(39):8618–24.
[33] Liu W, Geng L, Wu J, Huang An, Peng X. Highly strong and sensitive bilayer hydrogel actuators enhanced by cross-oriented nanocellulose networks. Compos Sci Technol 2022;225:109494.
[34] Gao JS, Zhao XX, Wen JP, Hu DT, Li RL, Wang K. Chinese calligraphy inspired design of humidity/light dual responsive magic paper. Adv Mater Technol 2021;6(8):2100044.
[35] Ma H, Jiang Y, Han W, Li X. High wet-strength, durable composite film with nacre-like structure for moisture-driven actuators. Chem Eng J 2023;457:141353.
[36] Zhang LD, Liang HR, Jacob J, Naumov P. Photogated humidity-driven motility. Nat Commun 2015;6:7429.
[37] Liu W, He Y, Leng J. Humidity-responsive shape memory polyurea with a high energy output based on reversible cross-linked networks. ACS Appl Mater Interfaces 2023;15(1):2163–71.
[38] Guo R, Zhang Q, Wu Y, Chen H, Liu Y, Wang J, et al. Extremely strong and tough biodegradable poly(urethane) elastomers with unprecedented crack tolerance via hierarchical hydrogen-bonding interactions. Adv Mater 2023;35(21).
[39] Yang S, He Y, Leng JS. Regulated photo/thermal dual and programmable staged responsive shape memory poly(aryl ether ketone). J Appl Polym Sci 2023;140(38).
[40] Li J, Mou L, Zhang R, Sun J, Wang R, An B, et al. Multi-responsive and multi-motion bimorph actuator based on super-aligned carbon nanotube sheets. Carbon 2019;148:487–95.
[41] de Groot JH, van Leeuwen JL. Evidence for an elastic projection mechanism in the chameleon tongue. Proc Royal Soc B 2004;271(1540):761–70.
[42] Chang L, Wang D, Huang Z, Wang C, Torop J, Li B, et al. A versatile ionomer-based soft actuator with multi-stimulus responses, self-sustainable locomotion, and photoelectric conversion. Adv Funct Mater 2023;33(6):2212341.
[43] Wang Z, Shi D, Wang X, Chen Y, Yuan Z, Li Y, et al. A multifunctional light-driven swimming soft robot for various application scenarios. Int J Mol Sci 2022;23(17):9609.
[44] Lin C, Huang Z, Wang Q, Zou Z, Wang W, Liu L, et al. Mass-producible near-body temperature-triggered 4D printed shape memory biocomposites and their application in biomimetic intestinal stents. Compos B Eng 2023;256:110623.
[45] Lan X, Liu LW, Liu YJ, Leng JS. Thermomechanical properties and deformation behavior of a unidirectional carbon-fiber-reinforced shape memory polymer composite laminate. J Appl Polym Sci 2019;137(14):48532.